Cryogenic transimpedance amplifier for micromechanical capacitive sensors

Article *in* The Review of scientific instruments · September 2008

DOI: 10.1063/1.2970944 · Source: PubMed

4 authors, including:

Pedro Julian
Universidad Nacional del Sur
131 PUBLICATIONS **1,262** CITATIONS

Cryogenic transimpedance amplifier for micromechanical capacitive sensors

D. Antonio,[1,a)] H. Pastoriza,[1,a)] P. Julián,[2,a)] and P. Mandolesi[2,b)]
[1]*Centro Atómico Bariloche, 8400 S. C. de Bariloche, Argentina*
[2]*Departamento de Ingenieria Eléctrica y Computadoras, Universidad Nacional del Sur, 8000 Bahía Blanca, Argentina*

(Received 29 May 2008; accepted 25 July 2008; published online 19 August 2008)

We developed a cryogenic transimpedance amplifier that works at a broad range of temperatures, from room temperature down to 4 K. The device was realized with a standard complementary metal oxide semiconductor 1.5 μm process. Measurements of current-voltage characteristics, open-loop gain, input referred noise current, and power consumption are presented as a function of temperature. The transimpedance amplifier has been successfully applied to sense the motion of a polysilicon micromechanical oscillator at low temperatures. The whole device is intended to serve as a magnetometer for microscopic superconducting samples. © *2008 American Institute of Physics.* [DOI: 10.1063/1.2970944]

I. INTRODUCTION

The study of phase transitions in confined systems, such as the nucleation of superconductivity in mesoscopic samples, has attracted a lot of interest lately because of the dramatic modification of the physical properties as sizes are reduced below certain characteristic lengths (the coherence length and penetration depth in the case of mesoscopic superconductors). Detecting the very small signals produced by this type of samples is a challenging task for experimentalists and new sensing devices often need to be designed.[1–5]

The purpose of this work is to develop the readout electronics for a Si micromechanical resonator used to measure magnetic properties in mesoscopic superconducting samples.[6] Having both small size and high Q, this resonator allows the detection of small torques, associated with changes in the magnetic moment, that are below the sensitivity of traditional instruments such as superconducting quantum interference device magnetometers. The resonator motion is capacitively sensed and the amplifying electronics must be capable of detecting very small capacitance variations, in the order of the femtofarads.

Capacitive detection is a technique broadly used in microelectrical mechanical systems. It offers low power, high sensitivity, and relatively easy implementation. However there are difficulties associated with capacitive detection such as high impedance, parasitics, electromagnetic interference (EMI), and cross-talk when electrostatic actuation is used.[7–9]

In cryogenic experiments long wires are needed to connect a sensor inside a dewar to the external electronics. The parasitic stray capacitances and the electromagnetic pickup noise introduced by these wires can be unacceptable when measuring very small capacitance variations. In these cases it is necessary to install the amplifier as close to the sensor as possible.[10]

The study of electronic systems operating at low temperatures has been carried out for decades and a special attention has been given to devices of the field effect transistor (FET) family, given that bipolar transistors fail to operate at temperatures below about 100 K.[11]

Silicon complementary metal oxide semiconductor (CMOS) transistors operated at low temperatures exhibit several advantageous characteristics such as increased carrier mobility, latch-up immunity, and reduced thermal noise. Nevertheless a number of problems such as impurity freeze-out and kink behavior are related to the operation at low temperatures.[12] Commercially available devices will generally fail or need special operating conditions at low temperatures.[13] The foundry usually provides physical process information such as gate oxide thickness, doping concentration, or channel mobility. It also provides empirical model parameters for circuit simulators such as the industry standard SPICE.[14] These parameters are extracted from carefully measured devices at room temperature, but generally cannot be extrapolated to very low temperatures. In this case parameter extraction needs to be performed again for a model that represents the region of operation of the device.

In this work we developed a two-stage unbuffered CMOS operational amplifier with a p-channel MOSFET differential input stage. First, we present the transimpedance amplifier as a suitable capacitive detector for the micromechanical resonator. Next, we describe the different stages of the design: transistor parameter extraction from low temperature measurements, circuit topology, required specifications, and determination of operating currents and transistor sizes. Finally, we evaluate the performance of the cryogenic transconductance amplifier measuring the mechanical frequency response of the microresonator at different temperatures.

[a)]Also at Consejo Nacional de Investigaciones Científicas y Técnicas (CONICET), CP C1033AAJ Buenos Aires, Argentina.
[b)]Also at Comisión de Investigaciones Científicas de la Provincia de Buenos Aires, Argentina.

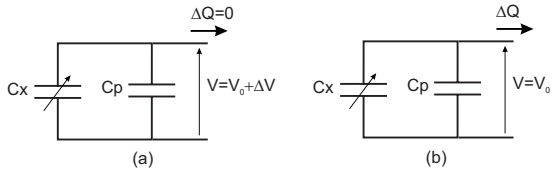

FIG. 1. Different configurations used in electrical capacitance detection. A variation ΔC_x in the capacitance C_x produces a variation ΔV in the output voltage V or a variation ΔQ in the total charge Q. In (a) charge is kept constant (measurement device with infinite input impedance) and $V=Q/C$ and $\Delta V=-V_0(\Delta C_x/C_p+C_x)$. In (b) voltage is kept constant (measurement device with zero input impedance) and $Q=CV$ and $\Delta Q=V\Delta C_x$. The advantage of the second approach is that the output does not depend on the parasitic capacitances represented by C_p.

II. TRANSIMPEDANCE AMPLIFIER

There are two main approaches for the electrical measurement of capacitance variation. The first approach consists of keeping charge in the capacitor constant and measuring variations of voltage and the second approach consists of keeping voltage constant and measuring variations of charge.[15] These two approaches and their response to capacitance variations are represented in the schematics of Fig. 1, where the stray parasitic capacitances are represented by C_p. The important advantage of measuring charge is that the response is not affected by parasitic capacitances if voltage in the capacitor is kept constant.

An implementation of the second approach can be made with a transimpedance amplifier, as shown in Fig. 2. One plate of the capacitor is connected to the ground and the other is held at a constant voltage V_b by the operational amplifier, through the feedback impedance Z_f. This constant voltage reduces the effect of the parasitics.

The output V_0 is proportional to the capacitance variation δC_x, to the feedback impedance Z_f, and to the bias voltage V_b. The total input capacitance inserts a zero in the transfer function and the capacitor C_f is needed in order to introduce a compensating pole. This capacitor limits the bandwidth of the circuit and its value should be optimized to stabilize the circuit while keeping the bandwidth within the required specifications.

III. AMPLIFIER DESIGN

The specifications for the design have been determined by the sensor requirements. The micromechanical oscillator

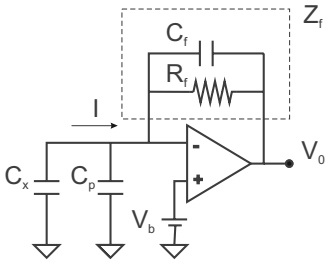

FIG. 2. Circuit diagram of the transimpedance amplifier. The negative feedback keeps voltage in the capacitor constant and equal to V_b. This is an implementation of the capacitance measuring approach described in Fig. 1(b). The output V_0 is proportional to V_b, Z_f, and δC_x but does not depend on the parasitic capacitances represented by C_p.

resonant frequency is approximately 50 KHz and the maximum voltage that can be applied between the fixed electrodes and the moving plate is about 10 V to avoid pull-in.[16] The load capacitance is given by cable capacitances and the input capacitance of the following amplifier stage.

In order to have an open-loop gain $A=40$ dB at the mechanical resonant frequency, the dc gain specification was set to $A_0=3000$ with a gain bandwidth GB=4 MHz. For the bias voltage V_b we decided that a 1.5 V battery would provide a noise-free biasing voltage, within the oscillator stable range limits. A supply voltage of 5 V was chosen to power the device and a slew rate of 1 $V/\mu s$ was considered suitable for the design.

A. Transistor characterization and parameter extraction

Given that the foundry only provides process parameter information at room temperature (300 K), the basic CMOS parameters are needed to be investigated at low temperatures. For this purpose we used two available parallel arrays of 1008 *n*-type MOS (NMOS) and 1008 *p*-type MOS (PMOS) transistors, respectively. These transistors belonged to the same fabrication process to be used for the operational amplifier fabrication. The advantage of using two arrays of small basic transistors instead of two large single transistors is that in the design every transistor can be built with series or parallel combinations of these basic transistors. Therefore all the transistors used in the design are the same than those used in the characterization measurements. The current-voltage characteristics of the MOSFETs were measured at different temperatures in vacuum inside a closed cycle APD Cryogenics HC-2 cryogenerator where the temperature can be varied between 23 and 300 K. The following simple model[17] was then used to fit the output I_{DS} versus V_{DS} and transfer I_{DS} versus V_{GS} curves:

$$I_{DS}=\frac{KW}{2L}(V_{GS}-V_t)^2(1+\lambda V_{DS}), \tag{1}$$

with $K=\mu_0 C_{ox}(W/L)$ where μ_0 is the surface mobility of the channel in $(cm^2/V\ s)$, C_{ox} is the capacitance per unit area of the gate oxide in (F/cm^2), W and L are the effective channel width and length, and λ is the channel length modulation parameter in (V^{-1}). Parameters K and V_t were obtained by taking the square root from I_{DS} versus V_{GS}, and then applying a least-squares linear fit. The Early voltage $V_A=1/\lambda$ was obtained from the I_{DS} versus V_{DS} curves as the point where the tangent to the saturation curve intersects the V_{DS} axis. The output resistance is

$$r_0=\frac{1}{\lambda I_{DS}}=\frac{V_A}{I_{DS}}. \tag{2}$$

The temperature dependence of the obtained parameter values is shown in Fig. 3. The parameter K increases as the temperature decreases from 120 K to approximately 40 K because the surface mobility increases. This is due to the fact that the lattice thermal energy decreases and the thermal scattering of carriers is reduced. For lower temperatures the mobility decreases due to the increase in nonthermal scattering processes such as those involving ionized impurities.[18]

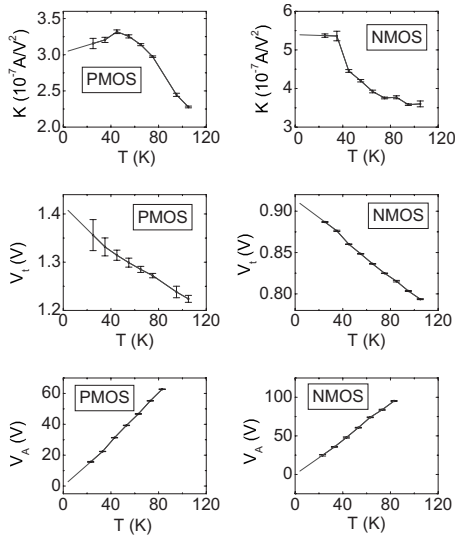

FIG. 3. PMOS and NMOS parameters as a function of temperature. The amplifier was designed considering a simple model for the transistors working in saturation where $I_{DS}=(KW/2L)(V_{GS}-V_t)^2(1+\lambda V_{DS})$. Parameters K, V_t, and $V_A=1/\lambda$ were extracted from the output I_{DS} vs V_{DS} and transfer I_{DS} vs V_{GS} curves.

The threshold voltage increases monotonically with decreasing temperature mainly due to the temperature dependence of the bulk Fermi level with temperature.[18,19] Finally, the Early voltage decreases with decreasing temperature, in agreement with previous results.[18]

B. Two-stage unbuffered operational amplifier

The chosen amplifier circuit topology is shown in Fig. 4. It consists of a two-stage differential amplifier with unbuffered output. The differential input was made with PMOS instead of NMOS transistors because they present lower flicker type noise[20] and less anomalous current-voltage characteristics at low temperatures.[21] Additionally, as a n-well process is being used and both M1 and M2 are PMOS their source and bulk terminals can be connected together and the source of M5 can be connected to its own bulk terminal. If these transistors were PMOS their bulk terminals would be

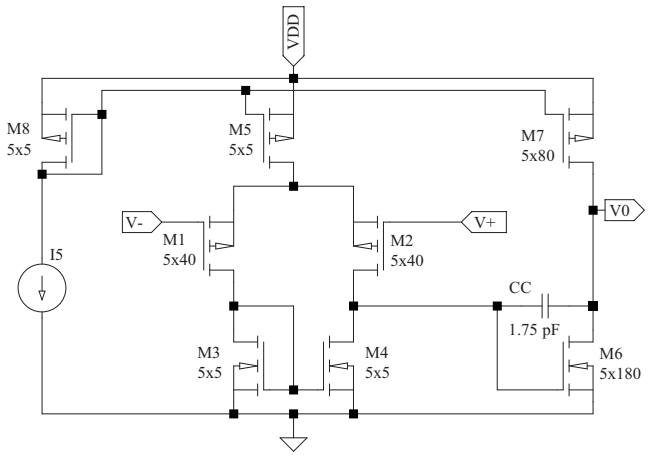

FIG. 4. Schematic for the two stage unbuffered operational amplifier. M1 and M2 form the p-channel differential input pair. CC is a compensation capacitor for improving stability of the circuit. I5 is an external current source.

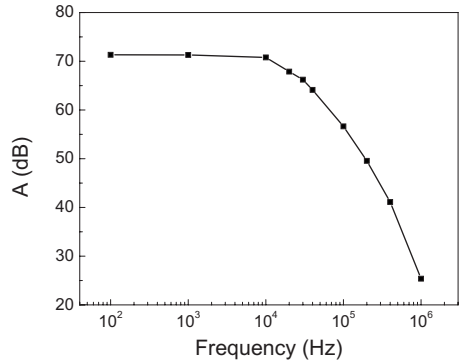

FIG. 5. Open loop gain vs frequency at 23 K. The dc gain is $a_0 \approx 71$ dB. The gain bandwidth is approximately 4 MHz. The two poles corresponding to the two amplifier stages are located at $p_1 \approx 20$ KHz and $p_2 \approx 300$ KHz.

connected together through the p-substrate, and both M1 and M2 would suffer the backgate effect[22] (source not connected to bulk and threshold voltage dependence on the backgate bias voltage).

With the specifications already described and the extracted CMOS parameter values, we calculated the different transistor sizes and operating currents. A description of the design process can be found in Ref. 17. The resulting transistor sizes were $(L \times W)$ as follows: M1 and M2: 5×40 μm^2, M3–M5: 5×5 μm^2, M6: 5×180 μm^2, M7: 5×80 μm^2, and M8: 5×5 μm^2.

The amplifier was made with a n-well CMOS standard process, with two metal layers, two polysilicon layers and poly-on-poly-capacitors. The final layout consisted of 34 PMOS and 38 NMOS transistors, each measuring 5×5 μm^2. These transistors were identical to the ones used in the characterization measurements. A value of 500 KΩ was chosen for the polysilicon feedback resistance R_f, which is large enough to have a good gain and with a practical value for circuit integration.

IV. PERFORMANCE MEASUREMENT

The open-loop gain, power consumption, and output noise voltage were characterized at different temperatures. For the open-loop gain measurement a 0.1 mVp.p. sine wave with a 1.5 V dc offset signal was applied to the noninverting input of the amplifier through a 120–1 voltage divider. Figure 5 shows the curve obtained at $T=23$ K, the minimum temperature reachable with this cryogenerator. The dc gain $a_0 \approx 71$ dB meets the design specification. The gain bandwidth is approximately 4 MHz as designed but the two amplifier gain dominant pole frequencies do not comply well to the design. Considering a second order model, each stage of the amplifier contributes with a pole in the open-loop gain.[17] The frequency of each pole can be obtained from the circuit parameter values using the following equations:

$$p_1 \approx \frac{(I_5/2)(\lambda_2+\lambda_4)I_6(\lambda_6+\lambda_7)}{g_{m6}Cc} \approx 1.4 \text{ KHz}, \quad (3)$$

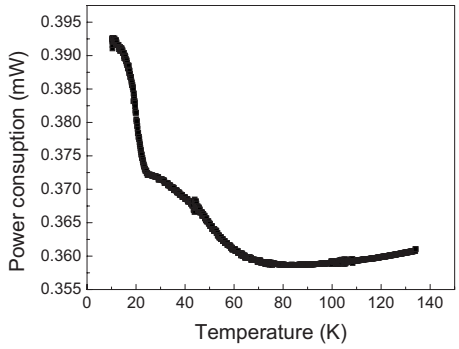

FIG. 6. Transimpedance amplifier power consumption as a function of temperature. The sensor is connected to the amplifier but with its input terminal connected to ground (no capacitance variation).

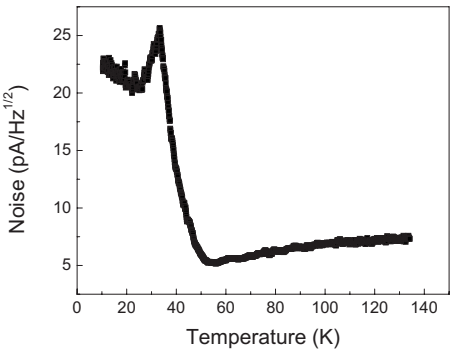

FIG. 7. Transimpedance amplifier input referred noise as a function of temperature. The sensor is connected to the amplifier but with its input terminal connected to ground (no capacitance variation).

$$p_2 \approx \frac{g_{m6}Cc}{C_1C_2 + C_2Cc + C_1Cc} \approx 4.5 \text{ MHz}, \quad (4)$$

where C_1 and C_2 are the capacitances to ground seen from the output of the first and second stage, respectively. These are the frequencies calculated from the parameter values assumed in the design. The pole frequencies obtained from Fig. 5 were $p_1 \approx 20$ KHz and $p_2 \approx 300$ KHz. This difference could be due to an error in the estimation of certain parameter values at low temperatures, such as an overestimation of the Early voltage. However, we compared the open-loop gain curves measured at room temperature with simulated curves (using the foundry extracted process parameters) and similar differences in the pole frequencies were also found. Therefore these frequency shifts are probably introduced by the capacitance of the different bonding pads that were included in the layout for testing purposes.

The low values of liquid helium density and latent heat of vaporization make it important to keep power dissipation low inside the dewar to maintain reasonable vaporization rates. Our cryogenic equipment has a heat in-leak in the order of tens of milliwatts and the electronic power dissipation should be kept below this value. The amplifier was designed to dissipate less than 1 mW and this value was verified experimentally. The power consumption was measured with a picoammeter in series with the power source. The amplifier was connected to the sensor output in the transimpedance configuration and the sensor input was connected to ground. Figure 6 shows the power consumption of the amplifier as a function of temperature. The increase in power consumption as temperature decreases is compatible with the increase in carrier mobility.

In our case the main motivation to develop low temperature electronics is to increase the sensor sensitivity. Therefore noise is a key concern. At low temperatures nonthermal noise such as flicker $(1/f)$-type noise can become important. It arises from processes such as random charge carrier trapping in the silicon substrate/gate oxide interface and can drastically increase when lowering the temperature.[23] The noise was registered with an EG&G 5302 lock-in amplifier which provides a measure of the root-mean square value of the output channel at the reference frequency and with a known equivalent noise bandwidth. The amplifier was connected to the sensor output in the transimpedance configuration and the sensor input was connected to ground. The reference frequency was set to 55KHz, which is the micromechanical oscillator resonance frequency. The amplifier input referred noise value was obtained by dividing the measured noise by the amplifier gain at that frequency and it is shown in Fig. 7 as a function of temperature. As can be seen, there is an initial decrease between 140 and 50 K probably associated with the reduction of thermal noise. Below 50 K there is a sharp increase in noise which peaks at about 26 $\text{pA}/\sqrt{\text{Hz}}$. In this temperature range, carrier freeze-out occurs, producing kink effects in the saturation region which may be related to an increase in noise.

V. APPLICATION TO MICRORESONATOR DETECTION

The transimpedance amplifier and the micromechanical resonator were connected together inside the vacuum can of a liquid helium cryostat. A function generator was then used to actuate the micromechanical resonator with different voltages and at different excitation frequencies.

Several frequency sweeps were recorded at different temperatures in order to investigate the frequency response of the micromechanical device. The capacitance variation amplitude of the resonator proportional to the mechanical oscillation amplitude produced signals well above the amplifier noise level. The mechanical resonance curves are shown in Fig. 8.

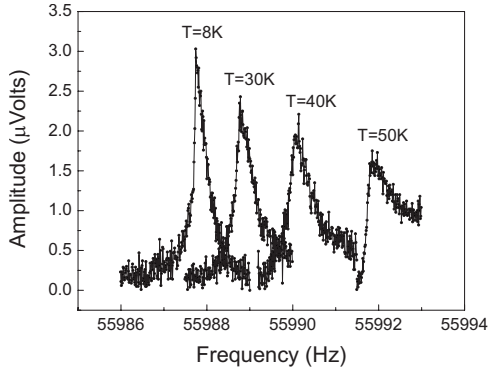

FIG. 8. Micromechanical oscillator resonance curves. A 2 mVp.p. sine wave with a 1 mV dc offset was applied to the sensor input terminal. Frequency sweeps were performed to find the torsional mode resonant frequency of the oscillator at different temperatures: 8, 30, 40, and 50 K.

The amplifier worked well through all the range of temperatures from room temperature to 4 K. Power consumption was low enough to allow good temperature control of the micromechanical resonator. Moreover, no increase in the rate of liquid helium evaporation was detected after the installation of the amplifier inside the cryostat.

[1] A. K. Geim, I. V. Grigorieva, S. V. Dubonos, J. G. S. Lok, J. C. Maan, A. Filippov, and F. Peeters, Nature (London) **390**, 259 (1997).
[2] C. A. Bolle, V. Aksyuk, F. Pardo, P. L. Gammel, E. Zeldov, E. Bucher, R. Boie, D. J. Bishop, and D. R. Nelson, Nature (London) **399**, 43 (1999).
[3] V. A. Schweigert, F. M. Peeters, and P. S. Deo, Nature (London) **81**, 2783 (1998).
[4] A. R. de C. Romaguera, M. M. Doria, and F. M. Peeters, Phys. Rev. B **76**, 020505 (2007).
[5] I. V. Grigorieva, W. Escoffier, J. Richardson, L. Y. Vinnikov, S. Dubonos, and V. Oboznov, Phys. Rev. Lett. **96**, 077005 (2006).
[6] M. Dolz, D. Antonio, and H. Pastoriza, Physica B (Amsterdam) **398**, 329 (2007).
[7] S. D. Senturia, *Microsystem Design* (Kluwer, Dordrecht, 2001).
[8] N. Yazdi, H. Kulah, and K. Najafi, Third IEEE International Conference on Sensors, Vienna, Austria, 2004 (unpublished), pp. 28–31.
[9] B. E. Boser, Transducers '97, 1997 International Conference on Solid State Sensors and Actuators, Chicago, 1997 (unpublished), pp. 1169–1172.
[10] P. Horowitz and W. Hill, *The Art of Electronics*, 2nd ed. (Cambridge University Press, Cambridge, England, 1989).
[11] R. Kirschman, Cryogenics **25**, 115 (1985).
[12] F. Balestra and G. Ghibaudo, *Device and Circuit Cryogenic Operation for Low Temperature Electronics* (Kluwer, Dordrecht, 2001).
[13] J. T. Hastings and K. W. Ng, Rev. Sci. Instrum. **66**, 3691 (1995).
[14] EECS Department of the University of California, The SPICE page (http://bwrc.eecs.berkeley.edu/Classes/icbook/SPICE/).
[15] G. K. Wong, in *Experimental Techniques in Condensed Matter Physics at Low Temperatures*, Frontiers in Physics, edited by R. C. Richardson and E. N. Smith (Addison-Wesley, Reading, MA, 1988), Chap. 4.
[16] H. C. Nathanson, W. E. Nevel, R. A. Wickstrom, and J. R. Davis, Jr., IEEE Trans. Electron Devices **14**, 117 (1967).
[17] P. Allen and D. Holberg, *CMOS Analog Circuit Design* (Oxford University Press, Oxford, 1987).
[18] S. K. Tewksbury, IEEE Trans. Electron Devices **28**, 1519 (1981).
[19] R. Wang, J. Dunkley, T. A. DeMassa, and L. F. Jelsma, IEEE Trans. Electron Devices **18**, 386 (1971).
[20] B. Razavi, *Design of Analog CMOS Integrated Circuits* (McGraw-Hill, New York, 2001).
[21] H. Nagata, H. Shibai, T. Hirao, T. Watabe, M. Noda, Y. Hibi, M. Kawada, and T. Nakagawa, IEEE Trans. Electron Devices **51**, 270 (2004).
[22] S. Liu, J. Kramer, G. Indiveri, T. Delbrück, and R. Douglas, *Analog VLSI: Circuits and Principles* (MIT, Cambridge, MA, 2002).
[23] S. Sesnic and G. Craig, IEEE Trans. Electron Devices **19**, 933 (1972).